Structures of electrosprayed Pb(Uracil−H) + complexes by infrared multiple photon dissociation spectroscopy

ARTICLE *in* INTERNATIONAL JOURNAL OF MASS SPECTROMETRY · DECEMBER 2011

Impact Factor: 1.97 · DOI: 10.1016/j.ijms.2011.04.003

2 AUTHORS:

Osama Y Ali
Memorial University of Newfoundland
6 PUBLICATIONS **42** CITATIONS
SEE PROFILE

Travis D Fridgen
Memorial University of Newfoundland
67 PUBLICATIONS **1,150** CITATIONS
SEE PROFILE

International Journal of Mass Spectrometry 308 (2011) 167–174

Contents lists available at ScienceDirect

International Journal of Mass Spectrometry

journal homepage: www.elsevier.com/locate/ijms

Structures of electrosprayed Pb(Uracil-H)$^+$ complexes by infrared multiple photon dissociation spectroscopy

Osama Y. Ali, Travis D. Fridgen*

Department of Chemistry, Memorial University of Newfoundland, St. John's, NL A1B 3X7, Canada

ARTICLE INFO

Article history:
Received 2 March 2011
Received in revised form 2 April 2011
Accepted 5 April 2011
Available online 22 April 2011

Keywords:
IRMPD spectroscopy
Pb–Uracil
Hydrated complexes
Calculations
Infrared
Gas-phase ion structures

ABSTRACT

The structures of three ion molecule complexes of [Pb(Ura-H)]$^+$ have been explored by infrared multiple photon dissociation (IRMPD) spectroscopy in the gas phase. A complex of [Pb(Ura-H)]$^+$ with uracil, [Pb(Ura-H)(Ura)]$^+$, or the singly or doubly water solvated complexes, [Pb(Ura-H)(H_2O)]$^+$ and [Pb(Ura-H)(H_2O)$_2$]$^+$, have been irradiated with tunable infrared radiation in the N–H/O–H stretching region (3200–4000 cm^{-1}) to produce IRMPD spectra which were compared with IR spectra computed using B3LYP/6-31+G(d,p) for various isomers. In all cases, the computed spectra for the lowest energy structures agree very well with the experimental IRMPD spectrum. Results show that all complexes involved a [Pb(Ura-H)]$^+$ core which is deprotonated at N3 and has lead bound to either N3 and O4 or N3 and O2. Our results suggest that the [Pb(Ura-H)]$^+$ structure that is deprotonated at N1 and lead is bound to N1 and O2 is not an significant contributor to the electrosprayed complexes. [Pb(Ura-H)(Ura)]$^+$ was found to have a four-coordinate lead. The water molecules in [Pb(Ura-H)(H_2O)]$^+$ and [Pb(Ura-H)(H_2O)$_2$]$^+$ were determined to be directly coordinated to lead, the first also hydrogen bonded to one carbonyl oxygen.

1. Introduction

The DNA molecule is responsible for a number of crucial roles in biology including the storage and transfer of genetic information. Noncovalent interactions play a fundamental role in many scientific fields and these interactions allow metal ions to influence essential biological processes such as those involving DNA [1]. Like many biological molecules, the structure and regular function of DNA can be impacted, positively or negatively, by the presence of other molecules and ions. A significant amount of research has been devoted to studying the impact that metal ions have on biological systems such as RNA folding, stabilization, and activity [2–5] and have also shown the influential impact that metal ions have on biological molecules including their role in the nature and function of proteins, nucleic acids, and peptide hormones. Various metal ions interact with DNA and consequently, can manipulate its structure [6–11]. The effect that these ions have on DNA depends largely on their binding location [12] and can lead to, for example, stabilization or competition for hydrogen bonding. When metal ions bind with nucleic acid bases they interfere with hydrogen bond interactions between base pairs and provoke a subsequent disruption in the double helix [12–14]. Depending on their nature, structural changes in DNA induced by the metal ion can have profound effects on the transfer of genetic information.

Lead is a common metal ion known to invoke a damaging effect on biological homeostasis [15]. Therefore much literature has focused on its toxic effects on human health [15,16]. These harmful effects impact many major organs including the liver, heart and kidneys.

Sigel and co-workers have published many interesting papers focusing on the interactions of Pb^{2+} ions in aqueous solution with phosphate, phosphonates [17], and nucleotides [18,19]. On the other hand, other papers deal with the reactivity of Pb^{2+} with nucleobases in the gas phase [20,21]. The reactivity of lead (II) ions with uracil and thymine has been investigated by mass spectrometry in gas phase [20]. Positive-ion electrospray spectra showed that the doubly charged complexes dissociate to give a singly charged [Pb(nucleobase)-H]$^+$ when the nucleobase was uracil or thymine. This singly charged ion is the most abundant complex observed in the electrospray mass spectra and was studied by MS/MS. [Pb(Ura-H)]$^+$ and [Pb(Thy-H)]$^+$ both dissociate by elimination of isocyanic acid (HNCO), and the formation of [PbNCO]$^+$ ion. Salpin et al. [21] have also studied the interactions between lead (II) and thiouracil derivatives (2-thiouracil, 4-thiouracil, and 2,4-dithiouracil) which also form [Pb(nucleobase)-H]$^+$ ions (for numbering scheme for uracil see Scheme 1). MS/MS spectra were recorded at different collision energies revealing that the fragmentation of 2-thiouracil is different than 4-thiouracil. The 2-thiouracil complex loses predominantly PbS while both 4-thiouracil and 2,4-dithiouracil lose

* Corresponding author. Tel.: +1 709 864 8083.
E-mail address: tfridgen@mun.ca (T.D. Fridgen).

1387-3806/$ – see front matter © 2011 Published by Elsevier B.V.
doi:10.1016/j.ijms.2011.04.003

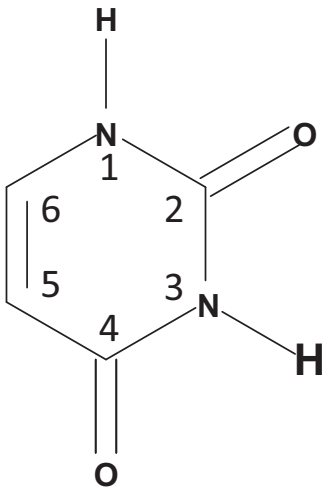

Scheme 1. Numbering scheme for uracil.

completely reduced Pb as the primary fragmentation route. The 2-thiouracil complex also loses HNCS while the 4-thiouracil complex loses HNCO. Even though the lowest energy structure in both has lead bound in a bidentate fashion to S and deprotonated N, a major fragmentation path, like in $[Pb(Ura\text{-}H)]^+$ and $[Pb(Thy\text{-}H)]^+$, involves breaking the N1–C2 bond and the N3–C4 bond.

It is important to determine ion structures in the gas phase without the complication from bulk solvent. One of the most common techniques to study structures of gaseous ions is infrared multiple photon dissociation (IRMPD) spectroscopy which has been revealing a number of surprises [22–24].

For instance, Atkins et al. [25] have studied the interactions of lead (II) ions with the glycine in the gas phase by using IRMPD spectroscopy in the N–H/O–H stretching region. Their results showed that the amino acid deprotonates at the amino group rather than the expected carboxylic acid group and lead coordinates to the deprotonated amino group and the carbonyl oxygen.

The present work has been conducted to determine the structure of gaseous complexes composed of a $[Pb(Ura\text{-}H)]^+$ core. It was not possible to investigate directly the $[Pb(Ura\text{-}H)]^+$ core due to a combination of its high dissociation energy and the low power of the laser used in these experiments. Three complexes involving the $[Pb(Ura\text{-}H)]^+$ core were investigated, $[Pb(Ura\text{-}H)(Ura)]^+$ composed of two uracils as well as the singly and doubly hydrated $[Pb(Ura\text{-}H)]^+$ complexes, $[Pb(Ura\text{-}H)(H_2O)]^+$ and $[Pb(Ura\text{-}H)(H_2O)_2]^+$.

2. Methods

2.1. Experimental

An ApexQe 70 Bruker Fourier Transform Ion Cyclotron Resonance (FT-ICR) coupled to a 10 Hz Nd:YAG pumped OPO (KTP, Euroscan) was used for this study. Details of the coupling of these two instruments will be presented in a forthcoming article. Uracil and lead nitrate were purchased from Sigma–Aldrich and used without any purification. Solutions of 1 mM uracil and 1 mM lead nitrate were prepared in 18 MΩ Millipore water. The solutions were introduced in the source using a syringe pump at flow rate of 100 μL/h. Electrosprayed ions were stored in the hexapole accumulation cell for 1–2 s prior to being transferred to the ICR cell. To solvate ions [26], the Ar flow to the hexapole cell was stopped and water vapour was allowed to flow into the hexapole cell. The ions are expected to have an ambient internal energy since they are stored in the hexapole for accumulation and/or solvation at $\sim 10^{-2}$ mbar.

Ions were irradiated by using the tunable infrared laser for 1–4 s. The more weakly bound and faster dissociating ions, i.e., the doubly hydrated, were irradiated for the shortest time, 1 s. Typically, the laser was scanned at 2 cm^{-1} intervals to produce the IRMPD spectra. The IRMPD efficiency is defined as the negative of the natural logarithm of the parent ion intensity divided by the sum of the fragment and parent ion signals.

2.2. Computational

Calculations were carried out by using Gaussian 09 suite of programs [27]. Structures were optimized and infrared spectra were calculated with the 6-31+G(d,p) basis set for C, H, N, and O atoms while the LANL2DZ basis set and relativistic core potential were used for the Pb atom. Single point MP2 calculations were performed on all the optimized structures using the same basis set and core potential for Pb and the 6-311++G(2d,p) basis sets on C, H, N, and O. This method is abbreviated MP2/6-311++G(2d,p)//B3LYP/6-31+G(d,p) in the rest of the paper and these calculations are used to compare the 298 K enthalpies and Gibbs energies of the isomeric species. The vibrational frequencies used to compute the zero-point energies and thermochemistries were unscaled. The infrared spectra were all scaled by a factor of 0.967 to compare with the experimental spectra. The predicted IR absorption bands are further convoluted by a Lorentzian function with a width (FWHM) of 10 cm^{-1} to compare with the experimental spectra.

3. Results and discussion

3.1. Comparison of IRMPD spectra of $[Pb(Ura\text{-}H)(Ura)]^+$, $[Pb(Ura\text{-}H)(H_2O)]^+$, and $[Pb(Ura\text{-}H)(H_2O)_2]^+$

The IRMPD dissociation pathways observed for the ions under study were as follows:

$$[Pb(Ura\text{-}H)(Ura)]^+ \xrightarrow{IRMPD} [Pb(Ura\text{-}H)]^+ + Ura$$

$$[Pb(Ura\text{-}H)(H_2O)]^+ \xrightarrow{IRMPD} [Pb(Ura\text{-}H)]^+ + H_2O$$

$$[Pb(Ura\text{-}H)(H_2O)_2]^+ \xrightarrow{IRMPD} [Pb(Ura\text{-}H)(H_2O)]^+ + H_2O$$

In the case of the latter, doubly hydrated $[Pb(Ura\text{-}H)]^+$, a second loss of water was also observed due to the absorption of the laser by the primary fragment ion.

The experimental IR spectra for $[Pb(Ura\text{-}H)(Ura)]^+$, $[Pb(Ura\text{-}H)(H_2O)]^+$, and $[Pb(Ura\text{-}H)(H_2O)_2]^+$ in the 3200–3900 cm^{-1} region are presented in Fig. 1. The spectrum of $[Pb(Ura\text{-}H)(Ura)]^+$ shows only a single sharp feature centred at 3485 cm^{-1} which can be assigned to N–H stretching vibrations. As there are expected to be at most three N–H bonds, such a simple spectrum might be indicative of a somewhat "symmetric" structure for this complex containing lead, uracil and a deprotonated uracil.

The spectrum for $[Pb(Ura\text{-}H)(H_2O)]^+$ is composed of only two sharp bands. One is centred at 3484 cm^{-1}, very similar to the band observed in the $[Pb(Ura\text{-}H)(Ura)]^+$ spectrum. The second band at 3701 cm^{-1} is most likely due to the water. Since there is only one absorption for the water molecule, it is quite likely that this is a free O–H stretch and the other O–H bond is involved in hydrogen bonding with the deprotonate uracil. The spectrum for $[Pb(Ura\text{-}H)(H_2O)_2]^+$ has the same two features as those observed for $[Pb(Ura\text{-}H)(H_2O)]^+$, centred at 3491 and 3718 cm^{-1}. A third sharp feature appears centred at 3637 cm^{-1}. A fourth, less prominent, but broad absorption is observed to occur at slightly higher energy, to the blue of the 3718 cm^{-1} feature.

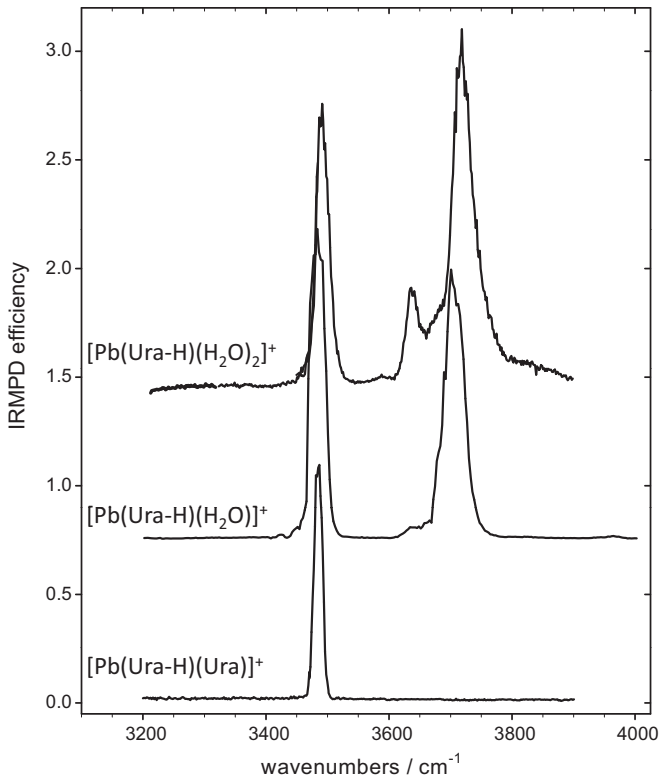

Fig. 1. Comparison of the IRMPD spectra of $[Pb(Ura-H)(Ura)]^+$, $[Pb(Ura-H)(H_2O)]^+$, and $[Pb(Ura-H)(H_2O)_2]^+$.

The C–H stretching vibrations are predicted to be weak and out of the range of the present experiment (<3200 cm^{-1}).

Each of these species and their structures will be discussed in turn, in the following sections.

3.2. $[Pb(Ura-H)(Ura)]^+$

In Fig. 2, eight of the lowest energy structures for $[Pb(Ura-H)(Ura)]^+$ are presented. The first four structures are similar in that lead is four-coordinate between two carbonyl oxygens and two deprotonated nitrogens. These first four lowest energy structures are all deprotonated at the most acidic nitrogen, N3 [28–33], of the left uracil. The right uracil of N3O4/N3O2 has seen a shift of the hydrogen from the N3 to O4 and there is a hydrogen bond between O4H of the right uracil and O2 of the left. Also, lead in N3O4/N3O2 is bound to deprotonated N3 and O4 of the left uracil and deprotonated N3 and O2 on the right ring. N3O4/N3O4 is almost identical except the hydrogen from N3 of the right uracil has been transferred to O2 which results in a hydrogen bond to O2 of the left ring and lead is, again, bound to deprotonated N3 and O4 of both uracils. N3O4/N3O2 is lower in Gibbs energy than the N3O4/N3O4 isomer, but only by 3.2 kJ mol^{-1} making them virtually isoenergetic. The next two structures, N3O2/N3O2 and N3O2/N3O4, are 7.7 and 8.0 kJ mol^{-1} higher in Gibbs energy, respectively, than the lowest energy structure. The right uracil in N3O2/N3O2 has seen the hydrogen from N3 shifted to O4, and a hydrogen bond between O4H of the right uracil and O4 of the left. In N3O2/N3O4, hydrogen has been shifted from N3 to O2 of the right hydrogen and the resulting O2H is hydrogen bound to O4 of the left uracil. Lead is bound to N3 and O2 of the right uracil in N3O2/N3O2 and to N3 and O4 of the right uracil in N3O2/N3O2.

As can be seen in Fig. 3, the predicted spectra for the lowest energy structures are almost identical in the 3200–3900 cm^{-1} region and both are in agreement with the experimental IRMPD spectrum. The observed and predicted bands are actually composed of two N–H stretching vibrations, but they are predicted to be only ~8 cm^{-1} separate from one another accounting for the observation and prediction of only one feature. The predicted spectra for N3O2/N3O2 and N3O2/N3O4 are identical to one another and that for the latter has been left out of Fig. 3 for clarity. The two N–H stretching vibrations for structure N3O2/N3O2 are predicted to be ~16 cm^{-1} apart, resulting in two slightly resolved bands. It is really

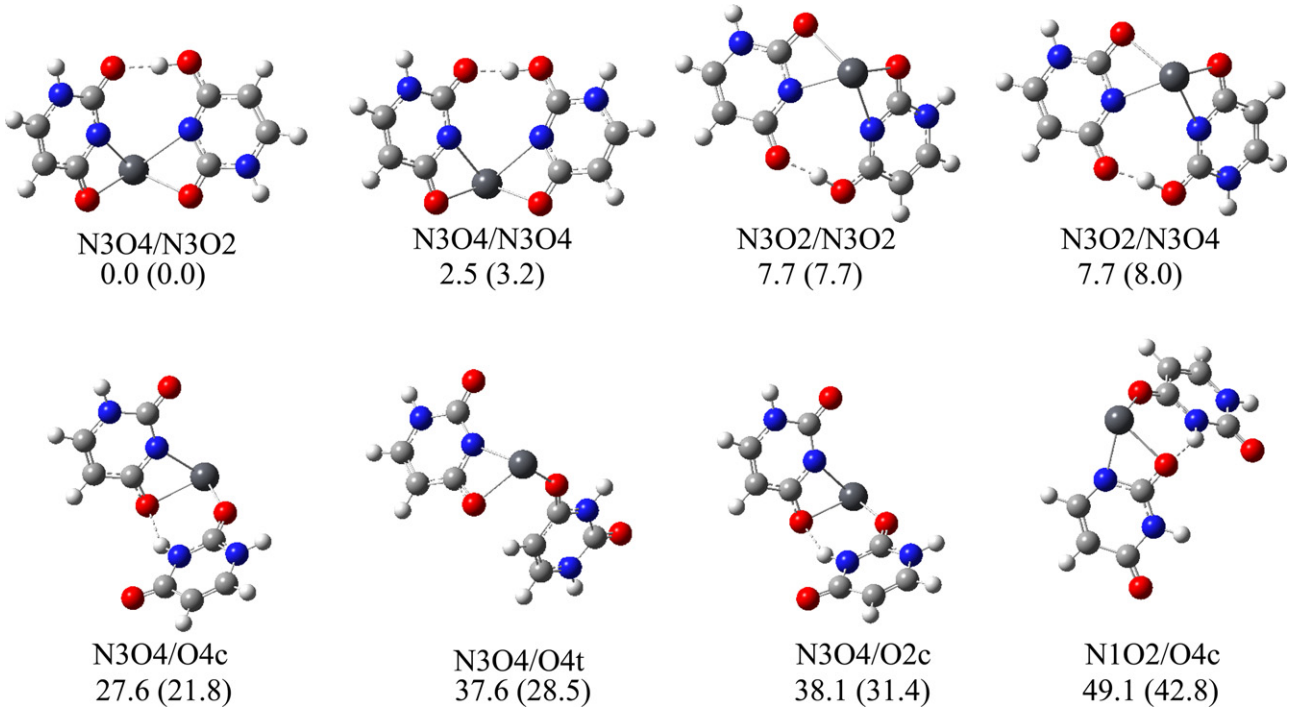

Fig. 2. Eight of the lowest-energy structures of $[Pb(Ura-H)(Ura)]^+$. 298 K relative enthalpies and Gibbs energies (in parentheses) reported in kJ mol^{-1} were calculated at the MP2/6-311++G(2d,p)//B3LYP/6-31+G(d,p) level of theory. All species have a single positive charge.

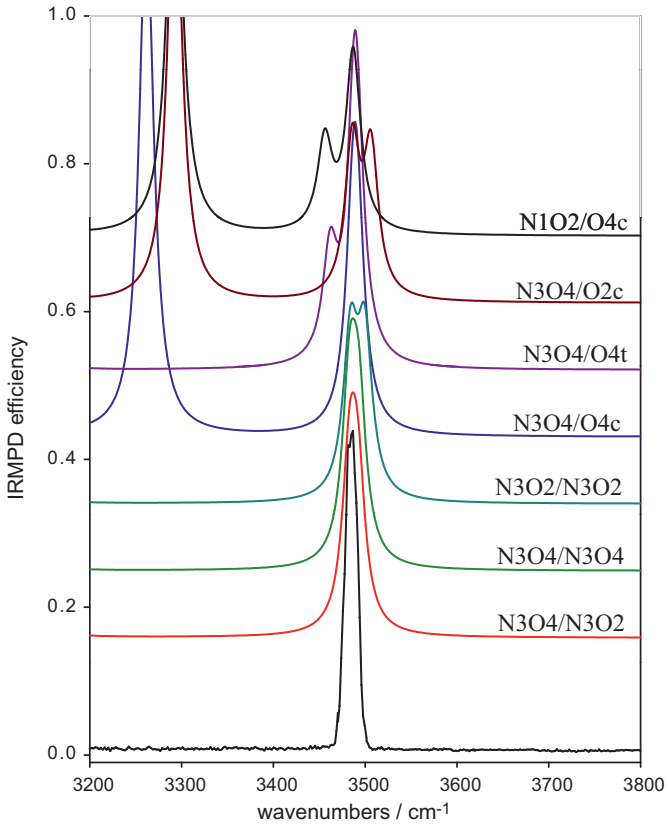

Fig. 3. Experimental IRMPD spectra of $[Pb(Ura\text{-}H)(Ura)]^+$ compared with B3LYP/6-31+G(d,p) spectra for $[Pb(Ura)(Ura\text{-}H)]^+$ structures shown in Fig. 2.

uncertain whether our laser could resolve these two bands, but we do note that the observed feature is quite sharp. For all three structures the hydrogen bond is strong resulting in shifts of the O–H stretch to below 2800 cm^{-1} in all cases, below the limit of the current laser in use. Spectroscopically the two lowest energy structures cannot be differentiated, and perhaps N3O2/N3O2 and N3O2/N3O4 cannot be differentiated either. However, N3O2/N3O2 and N3O2/N3O4 are unlikely candidates as a major contributors to the IRMPD spectrum based on their higher relative energies—they are predicted to be present in less than 1 part in 20 each compared to the lowest energy isomer.

The N3O4/O4c, N3O4/O4t and N3O4/O2c isomers (c and t refer to cis and trans—depending on whether uracil has an N–H bond or a C–H bond, respectively, pointing toward the $[Pb(Ura\text{-}H)]^+$ core), in Fig. 2, see lead binding in a three-coordinate fashion. In each lead binds to the N3 deprotonated nitrogen and O4 of the deprotonated uracil, and to one of the carbonyl oxygens on the second uracil. They are all higher in Gibbs energy by between 22 and 31 kJ mol^{-1} compared to the lowest energy structure which, on thermodynamic grounds, make them unlikely contributors to the observed spectrum. Isomers N3O4/O4c and N3O4/O4t have lead bound to O4 of the second uracil while in N3O4/O2c, it is bound to O2. Structures N3O4/O4c and N3O4/O2c have intramolecular hydrogen bonds between the two uracils. As seen in Fig. 3, these weak intramolecular hydrogen bonds result in a red-shift of the N–H stretch that is not observed experimentally. Similarly, the calculations predict different positions for the N–H stretches for N3O4/O4t and N3O4/O2c, but that is not observed experimentally. The lowest energy structure where uracil has been deprotonated at N1, N1O2/O4c is 42.8 kJ mol^{-1} higher in Gibbs energy than N3O4/N3O2. Based on energy it is unlikely to be a contributor to the spectrum, and spectroscopically it can be ruled out as well since the hydrogen bonded N–H stretch is not observed, nor are the multiple N–H stretches which are predicted by the calculations. There are many other structures as seen in Supplementary Fig. S1. All of them can be ruled out spectroscopically, and due to their thermochemistry relative to the lowest energy isomer.

3.3. $[Pb(Ura\text{-}H)(H2O)]^+$

Based on the experimental IRMPD spectrum, containing a feature in the N–H stretch region (3484 cm^{-1}) and one in the O–H stretch region (3701 cm^{-1}), the structure of $[Pb(Ura\text{-}H)(H_2O)]^+$ is most likely one in which we have the same lowest-energy $[Pb(Ura\text{-}H)]^+$ core as for $[Pb(Ura\text{-}H)(Ura)]^+$, discussed in the previous section, where uracil is deprotonated at the most acidic site [28–33], N3, so that the band at 3484 cm^{-1} is the N1–H stretch. Also, the position of the O–H stretch, 3701 cm^{-1}, is intermediate between where the free water symmetric and antisymmetric stretching vibrations (3657 and 3756 cm^{-1}, respectively) [34] might occur. The water is most likely participating in a hydrogen bond acting as a hydrogen bond donor. In Fig. 4, N3O4/wbO2 (wb means water is "bridged", or hydrogen bonded, in this case to O2) has lead bound to N3 and O4 and water bound to lead and acting as a hydrogen bond donor to O2. Slightly higher in energy, N3O2/wbO4 differs only in that lead is bound to O2 and water is hydrogen bonded to O4. As can be seen in Fig. 5, the computed IR spectra for both of these structures agree well with the experimental spectrum and it is impossible to distinguish between the two spectroscopically in the 3200–4000 cm^{-1} region. The band at 3701, is assigned to the free O–H stretch of water. Based on the relative thermochemistry, it is not expected that N3O2/wbO4 contributes to the experimental spectrum by more than 10% compared to N3O2/wbO2. The main difference which would allow spectroscopic differentiation might be the hydrogen bonded O–H stretch which is predicted to occur at 2825 and 2230 cm^{-1} for N3O2/wbO2 and N3O2/wbO4, respectively (Fig. S2). The huge difference is due to the hydrogen bond for structure N3O2/wbO4 being stronger since O4 is more basic than O2. The water bend is predicted to occur at 1572 and 1622 cm^{-1} for N3O2/wbO2 and N3O2/wbO4, respectively, and the out of phase C=O stretch is expected at 1534 and 1464 cm^{-1}, respectively, which could also be used to aid in distinguishing these two isomers (see Fig. S2).

N3O4/w is 7.1 kJ mol^{-1} higher in Gibbs energy than N3O4/wbO2 and also has water bound to lead but it is not participating in any hydrogen bonding. It is obvious from Fig. 5 that the predicted spectrum for this structure is not in agreement with the experimental IRMPD spectrum. Similarly, the tautomeric structures N1O2/wO4H and N1O2/w, which are much higher in energy due to being deprotonated at N1, can be ruled out spectroscopically. N3O4/wO2H is a tautomer of N3O4/w where hydrogen transferred from N1 to O2 and can be ruled out spectroscopically. Structure N3O4/wN1 is some 46 kJ mol^{-1} higher in Gibbs energy is the only structure considered where water is not bound to lead but is bound by a hydrogen bond to N1H. This results in the N1H stretch being red-shifted to 3115 cm^{-1} which is just beyond the useful output of our laser. The water symmetric and antisymmetric stretching vibrations, predicted to be at 3674 and 3791 cm^{-1}, respectively, are not observed. All but the two lowest energy isomers, N3O4/wbO2 and N3O2/wbO4, can be ruled out on spectroscopic and thermochemical grounds from being present in any significant amount.

3.4. $[Pb(Ura\text{-}H)(H_2O)_2]^+$

Like $[Pb(Ura\text{-}H)H_2O]^+$, the two lowest energy structures of $[Pb(Ura\text{-}H)(H_2O)_2]^+$ are based on lead bound either to deprotonated N3 and O4 or to deprotonated N3 and O2 (Fig. 6). Furthermore, N3O4/wbO2/w and N3O2/wbO4/w can be considered formed from

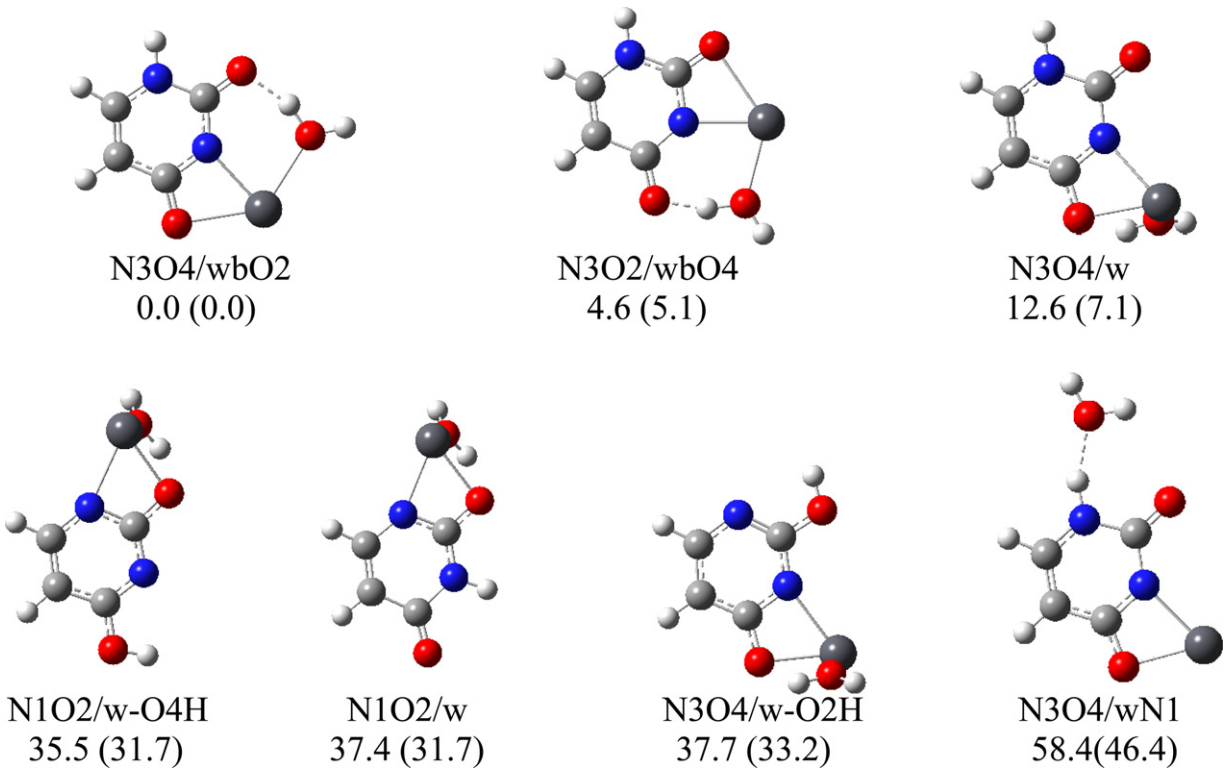

Fig. 4. Seven computed structures for $[Pb(Ura\text{-}H)(H_2O)]^+$. The 298 K MP2/6-311+G(2d,p)//B3LYP/6-31++G(d,p) relative enthalpies, and Gibbs energies (in parentheses) in kJ mol^{-1} are provided for each structure. All species have a single positive charge.

a water molecule adding to N3O4/wbO2 and N3O2/wbO4 in Fig. 4, respectively. The predicted infrared spectra of these two lowest energy complexes are identical in the 3200–3900 cm^{-1} region, and so cannot be differentiated spectroscopically in this region (see Fig. 7).

Do the calculated infrared spectra compare favourably with the experimental IRMPD spectrum? The resolved bands in the experimental IRMPD spectrum of $[Pb(Ura\text{-}H)(H_2O)_2]^+$ at 3491 and 3718 cm^{-1} can be assigned to the N–H stretch and the free O–H stretch of the water molecule that is bound to lead *and* hydrogen bonded to either O4 or O2. These assignments are the same as those made for $[Pb(Ura\text{-}H)(H_2O)]^+$. The band at 3637 cm^{-1} agrees quite well with the symmetric stretch of the out of plane water bound to lead in both N3O4/wbO2/w and N3O2/wbO4/w. The 3637 cm^{-1} band is also in a similar position to the symmetric O–H stretch of water bound to $Li(Ura)^+$ at 3635 cm^{-1} [35], to $Li(Thy)(Ade)^+$ at 3658 cm^{-1} [36], and to $M(Ade)^+$, where M is Li, Na, K (all ~3640 cm^{-1}) [37].

In the IRMPD spectrum there is also a broad absorption that grows more intense proceeding to the red of 3900 cm^{-1} and which can also be seen to contribute to IRMPD intensity between the 3718 and 3637 cm^{-1} bands. It has been observed in the past that the antisymmetric O–H stretch of water bound to metal ions observed by consequence spectroscopy is broadened and not nearly as intense as would be expected by an absorption spectroscopy measurement [35,38,39]. This phenomenon has been explained [39]. Briefly, consequence spectroscopies such as IRMPD spectroscopy rely on intramolecular vibrational-energy redistribution (IVR) following each photon absorption in order to be able to absorb multiple photons and cause dissociation. If there is not good IVR, then the mode is not available to absorb further photons. Anharmonic calculations for $Li(Ura)(H_2O)^+$ and $Li(Ura)(H_2O)_2^+$ predicted cubic coupling constants for the antisymmetric stretch can be as much as 3–4 orders of magnitude smaller than those for the symmetric stretch [35]. It is our premise that the antisymmetric O–H stretch predicted to

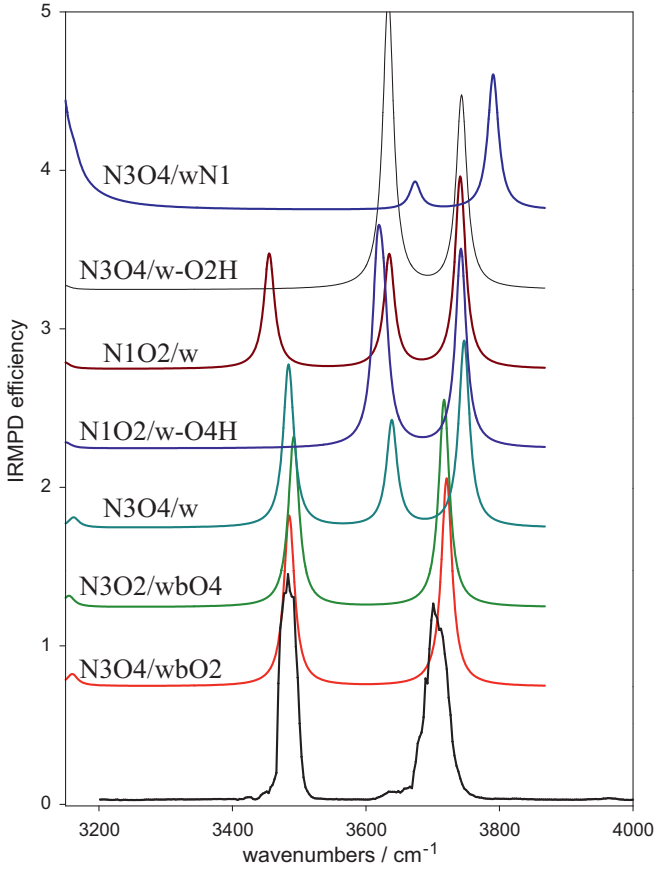

Fig. 5. Comparison of the experimental IRMPD spectrum for $[Pb(Ura\text{-}H)(H_2O)]^+$ and the predicted IR spectra for the computed structures in Fig. 4.

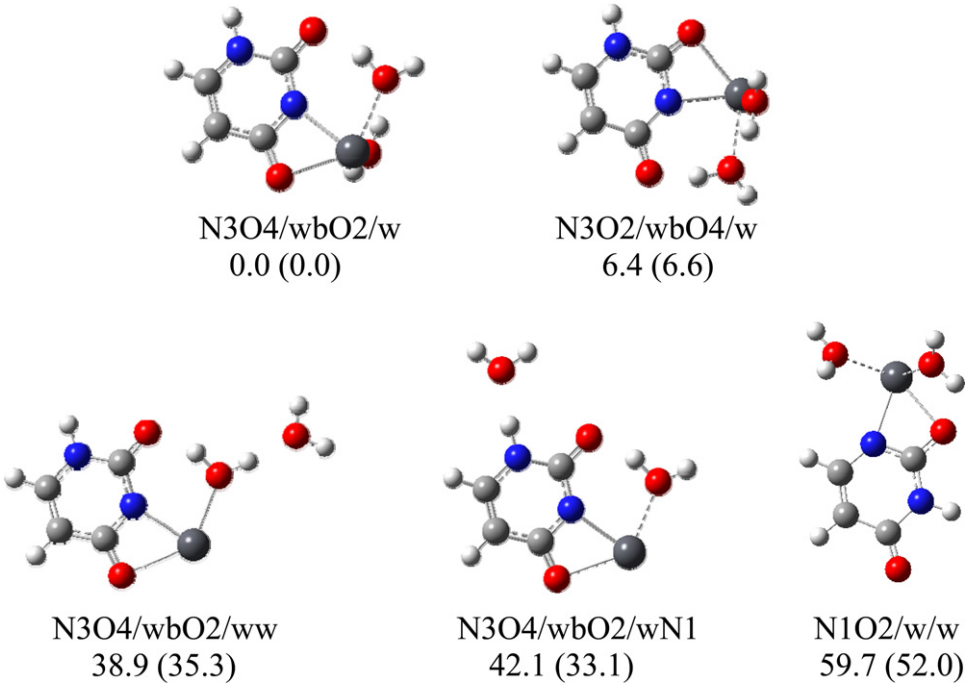

Fig. 6. B3LYP/6-31+G(d,p) structures of five $[Pb(Ura\text{-}H)(H_2O)_2]^+$ structures. The 298 K MP2/6-311++G(2d,p)//B3LYP/6-31+G(d,p) relative enthalpies and Gibbs energies (in parentheses) in kJ mol^{-1} are provided. All species have a single positive charge.

be at 3753 cm^{-1} is observed as IRMPD intensity between 3600 and 3900 cm^{-1} but is masked by the very intense free O–H stretch of the hydrogen bonded water. Furthermore, while we cannot rule out N3O2/wbO4/w spectroscopically, based on the calculated thermochemistry its presence is expected to be less than 8% than that of N3O4/wbO2/w at 298 K.

In N3O4/wbO2/ww and N3O4/wbO2/wN1, the second water is hydrogen bound as a hydrogen bond acceptor to either the first water or to N1H, respectively. These structures are considerably higher in energy than the two lower energy ones and are not expected to be present in any quantity measureable spectroscopy. N1O2/w/w is deprotonated at N1, lead is bound to N1 and O2, and both water molecules are bound to lead; it is a much higher energy structure. The computed infrared spectra for these three species are clearly not in agreement with the experimental IRMPD spectrum and can be ruled out as contributors.

A slight blue shift in the position of the free O–H stretch of the hydrogen bonded water molecule is observed between the singly and doubly solvated species, 3701 cm^{-1} $[Pb(Ura\text{-}H)(H_2O)]^+$ and 3718 for $[Pb(Ura\text{-}H)(H_2O)_2]^+$ and deserves discussion. This blue shift can be explained as the positive charge is shared not only by one water molecule as in $[Pb(Ura\text{-}H)(H_2O)]^+$, but also by two water molecules in $[Pb(Ura\text{-}H)(H_2O)_2]^+$. The simple Mulliken charge distribution shows that the water molecule in $[Pb(Ura\text{-}H)(H_2O)]^+$ has a charge of 0.126. Adding a second water molecule reduces the overall charge on the first to 0.071. This also results in a weaker and therefore elongated hydrogen bond, 1.597 Å vs. 1.642 Å, respectively, for the singly and doubly hydrated species. The extra electron density provided by the second water molecule in $[Pb(Ura\text{-}H)(H_2O)_2]^+$ results in a slightly stronger O–H bond of the first water molecule and a slight blue shift in the position of the vibrational mode.

3.5. Structure of $[Pb(Ura\text{-}H)]^+$

We were unable to obtain spectra for $[Pb(Ura\text{-}H)]^+$, likely due to the high energies required for dissociation. This is a limita-

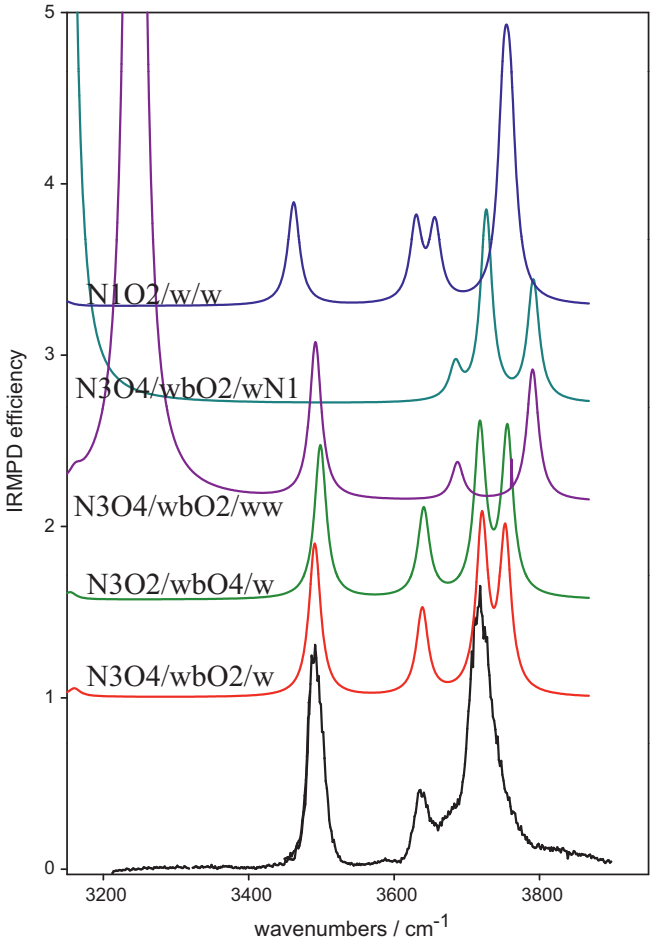

Fig. 7. The IRMPD spectrum for $[Pb(Ura\text{-}H)(H_2O)_2]^+$ in the 3200–3900 cm^{-1} range compared to the computed spectra for the five complexes shown in Fig. 6.

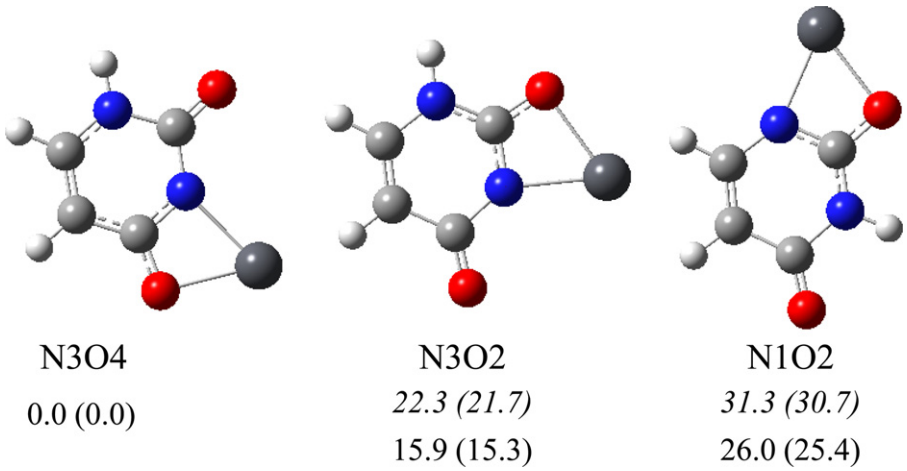

Fig. 8. Three lowest energy B3LYP/6-31+G(d,p) structures for $[Pb(Ura\text{-}H)]^+$. The 298 K MP2/6-311++G(2d,p)//B3LYP/6-31+G(d,p) relative enthalpies and Gibbs energies (in parentheses) as well as the B3LYP/6-31+G(d,p) energies (in italics top), all in kJ mol^{-1} are provided. All species have a single positive charge.

tioin of IRMPD spectroscopy, especially using a table-top OPO laser. However, our results, especially on $[Pb(Ura\text{-}H)(H_2O)]^+$ and $[Pb(Ura\text{-}H)(H_2O)_2]^+$ clearly show that there is no spectroscopic evidence for structures of these ions which contain the N1 deprotonated isomer with lead attached to N1 and O2 like N1O2 in Fig. 8. Remember that the hydrated ions are formed by storing electrosprayed $[Pb(Ura\text{-}H)]^+$ in the hexapole accumulation cell with a high pressure ($\sim 10^{-2}$ mbar of water vapour), which should be a fairly soft association process with many thermalizing collisions to soak up the energy of association. The three lowest energy structures of $[Pb(Ura\text{-}H)]^+$ are shown in Fig. 8. Based on the thermodynamics it is clear that N3O4 is by far the lowest energy complex being 15.3 kJ mol^{-1} lower in Gibbs energy than N3O2 at the MP2/6-311++G(2d,p)//B3LYP/6-31+G(d,p). The relative thermochemistries for these structures agree well with the previously reported B3LYP/6-311+G(3df,2p) calculations [20]. It is true that association of water tends to equalize the energies of the N3O4 and N3O2 "cores" as seen by the relative energies of structures N3O4/wbO2 and N3O2/wbO4 as well as N3O4/wbO2/w and N3O2/wbO4/w in Figs. 4 and 6, respectively. This is not true for the N1O2 core as seen by structures N1O2/w and N1O2/w/w in Figs. 4 and 6, respectively. Our experiments especially, as well as our calculations, suggest that the structure of $[Pb(Ura\text{-}H)]^+$ which is electrosprayed is that of N3O4.

Guillaumont et al. [20] studied the CID fragmentation of electrosprayed $[Pb(Ura\text{-}H)]^+$. The major dissociation routes observed were loss of isocyanic acid and the formation of $PbNCO^+$. Isotopic labeling studies also showed that isocyanic acid loss was exclusively loss of N3 and C2. The other major CID product ion, $PbNCO^+$, also exclusively includes N3 and C2. In order to explain these major CID products, isomers N3O2 and N1O2 (Fig. 8) were assumed to be present in the mixture of ions electrosprayed, even though their energies are substantially higher than N3O4.

Their calculations [20] of the potential energy surface showed that $PbNCO^+$ can be easily explained as arising from N3O2. Although the N3O2 isomer is significantly higher in energy than N3O4, under CID conditions, it is quite plausible that N3O2 can be formed as an intermediate from N3O4 *en route* to $PbNCO^+$. Isocyanic acid loss was only considered to be accessible through the N1O2 isomer which was said to be present in the mixture of electrosprayed ions. Our experiments do not support this conclusion in that we see no evidence for the N1O2 isomer, certainly not in enough abundance that the major dissociation route stems from it. It is not the intent of this work to explore the potential energy surface for $[Pb(Ura\text{-}H)]^+$ dissociation, but we suggest that there is probably an accessible route for N3O4 to lose HNCO under energetic CID conditions and would be consistent with the HNCO fragment coming from N3 and C2 of $[Pb(Ura\text{-}H)]^+$.

4. Summary

The structures of $[Pb(Ura\text{-}H)(Ura)]^+$, $[Pb(Ura\text{-}H)(H_2O)]^+$, and $[Pb(Ura\text{-}H)(H_2O)_2]^+$ have been explored using IRMPD spectroscopy in the N–H/O–H stretching region and by computational methods. In all cases, the computed spectra for the lowest energy structures agree very well with the experimental IRMPD spectrum. All these structures involved a $[Pb(Ura\text{-}H)]^+$ core which is deprotonated at N3 and has lead bound to either N3 and O4 or N3 and O2. Our results suggest that the $[Pb(Ura\text{-}H)]^+$ structure that is deprotonated at N1 and lead is bound to N1 and O2 is not an observable contributor to the electrosprayed complexes.

Acknowledgements

The authors acknowledge the financial contributions of the NSERC Discovery Grants program, the Canadian Foundation for Innovation, Memorial University, and Bruker Daltonics. We also would like to congratulate Professor Eyler on his retirement. The authors are also grateful for the very helpful comments from the reviewers.

Appendix A. Supplementary data

Supplementary data associated with this article can be found, in the online version, at doi:10.1016/j.ijms.2011.04.003.

References

[1] C. Ma Jennifer, D.A. Dougherty, The cation–π interaction, Chem. Rev. 97 (1997) 1303–1324.
[2] A.M. Pyle, Metal ions in the structure and function of RNA, J. Biol. Inorg. Chem. 7 (2002) 679–690.
[3] V.K. Misra, D.E. Draper, On the role of magnesium ions in RNA stability, Biopolymers 48 (1998) 113–135.
[4] R. Hanna, J.A. Doundna, Metal ions in ribozyme folding and catalysis, Curr. Opin. Chem. Biol. 4 (2000) 166–170.
[5] E. Madore, C. Florentz, R. Giege, J. Lapointe, Magnesium-dependent alternative foldings of active and inactive *Escherichia coli* tRNA(Glu) revealed by chemical probing, Nucleic Acids Res. 27 (1999) 3583–3588.
[6] X. Shui, C.C. Sines, L. McFail-Isom, D. VanDerveer, L.D. Williams, Structure of the potassium form of CGCGAATTCGCG: DNA deformation by electrostatic collapse around inorganic cations, Biochemistry 37 (1998) 16877–16887.

[7] G.L. Eichhorn, The effect of metal ions on the structure and function of nucleic acids, Adv. Inorg. Biochem. 3 (1981) 1–46.
[8] W.F. Dove, N. Davidson, Cation effects on the denaturation of deoxyribonucleic acid (DNA), J. Mol. Biol. 5 (1962) 467–478.
[9] G.L. Eichhorn, Y.A. Shin, Interaction of metal ions with polynucleotides and related compounds. XII. The relative effect of various metal ions on DNA helicity, J. Am. Chem. Soc. 90 (1968) 7323–7328.
[10] J. Sponer, J. Leszczynski, P. Hobza, Structures and energies of hydrogen-bonded DNA base pairs. A nonempirical study inclusion of electron correlation, J. Phys. Chem. 100 (1996) 1965–1974.
[11] J.V. Burda, J. Sponer, J. Leszczynski, P. Hobza, Interaction of DNA base pairs with various metal cations (Mg^{2+}, Ca^{2+}, Sr^{2+}, Ba^{2+}, Cu^{+}, Ag^{+}, Au^{+}, Zn^{2+}, Cd^{2+}, and Hg^{2+}): nonempirical ab initio calculations on structures, energies, and nonadditivity of the interaction, J. Phys. Chem. B 101 (1997) 9670–9677.
[12] W. Saenger, Principles of Nucleic Acid Structure, Springer-Verlag, New York, 1984.
[13] B.A. Cerda, C. Wesdemiotis, Li^{+}, Na^{+}, and K^{+} binding to the DNA and RNA nucleobases. Bond energies and attachment sites from the dissociation of metal ion-bound heterodimers, J. Am. Chem. Soc. 118 (1996) 11884–11892.
[14] L. McFail-Isom, C.C. Sines, L.D. Williams, DNA structure: cations in charge? Curr. Opin. Struct. Biol. 9 (1999) 298–304.
[15] R.A. Goyer, H.G. Seiler, H. Sigel, A. Sigel, Handbook on Toxicity of Inorganic Compounds, Dekker, New York, 1988.
[16] R.B. Martin, H.G. Seiler, H. Sigel, A. Sigel, Handbook on Toxicity of Inorganic Compounds, Dekker, New York, 1988.
[17] C.P. Da Costa, H. Sigel, Stabilities of complexes formed between lead(II) and simple phosphonate or phosphate monoester ligands including some pyrimidine-nucleoside 5′-monophosphates (CMP2-, UMP2-, dTMP2-), J. Biol. Inorg. Chem. 4 (1999) 508–514.
[18] C.P. Da Costa, H. Sigel, Lead(II)-binding properties of the 5′-monophosphates of adenosine (AMP^{2-}), inosine (IMP^{2-}), and guanosine (GMP^{2-}) in aqueous solution. Evidence for nucleobase–lead(II) interactions, Inorg. Chem. 39 (2000) 5985–5993.
[19] H. Sigel, C.P. Da Costa, R.B. Martin, Interactions of lead(II) with nucleotides and their constituents, Coord. Chem. Rev. 219 (2001) 435–461.
[20] S. Guillaumont, J. Tortajada, J.Y. Salpin, A.M. Lamsabhi, Experimental and computational study of the gas-phase interactions between lead(II) ions and two pyrimidic nucleobases: uracil and thymine, Int. J. Mass Spectrom. 243 (2005) 279–293.
[21] J.Y. Salpin, S. Guillaumont, J. Tortajada, A.M. Lamsabhi, Gas-phase interactions between lead(II) ions and thiouracil nucleobases: a combined experimental and theoretical study, J. Am. Soc. Mass Spectrom. 20 (2009) 359–369.
[22] J.R. Eyler, Infrared multiple photone diiociation spectroscopy of ions in Penning traps, Mass Spectrom. Rev. 28 (2009) 448–467.
[23] T.D. Fridgen, Infrared consequence spectroscopy of gaseous protonated and metal ion cationized complexes, Mass Spectrom. Rev. 28 (2009) 586–607.
[24] N.C. Polfer, J. Oomens, Vibrational spectroscopy of bare and solvated ionic complexes of biological relevance, Mass Spectrom. Rev. 28 (2009) 468–494.
[25] C.G. Atkins, L. Banu, M. Rowsell, V. Blagojevic, D.K. Bohme, T.D. Fridgen, Structure of $[Pb(Gly\text{-}H)]^{+}$ and the monosolvated water and methanol solvated species by infrared multiple-photon dissociation spectroscopy, energy-resolved collision-induced dissociation, and electronic structure calculations, J. Phys. Chem. B 113 (2009) 14457–14464.
[26] K. Rajabi, M.L. Easterling, T.D. Fridgen, Solvation of electrosprayed ions in the accumulation/collision hexapole of a hybrid Q-FTMS, J. Am. Soc. Mass Spectrom. 20 (2009) 411–418.
[27] M.J.T.G.W. Frisch, H.B. Schlegel, G.E. Scuseria, M.A. Robb, J.R. Cheeseman, J.A. Montgomery Jr., T. Vreven, K.N. Kudin, J.C. Burant, J.M. Millam, S.S. Iyengar, J. Tomasi, V. Barone, B. Mennucci, M. Cossi, G. Scalmani, N. Rega, G.A. Petersson, H. Nakatsuji, M. Hada, M. Ehara, K. Toyota, R. Fukuda, J. Hasegawa, M. Ishida, T. Nakajima, Y. Honda, O. Kitao, H. Nakai, M. Klene, X. Li, J.E. Knox, H.P. Hratchian, J.B. Cross, C. Adamo, J. Jaramillo, R. Gomperts, R.E. Stratmann, O. Yazyev, A.J. Austin, R. Cammi, C. Pomelli, J.W. Ochterski, P.Y. Ayala, K. Morokuma, G.A. Voth, P. Salvador, J.J. Dannenberg, V.G. Zakrzewski, S. Dapprich, A.D. Daniels, M.C. Strain, O. Farkas, D.K. Malick, A.D. Rabuck, K. Raghavachari, J.B. Foresman, J.V. Ortiz, Q. Cui, A.G. Baboul, S. Clifford, J. Cioslowski, B.B. Stefanov, G. Liu, A. Liashenko, P. Piskorz, I. Komaromi, R.L. Martin, D.J. Fox, T. Keith, M.A. Al-Laham, C.Y. Peng, A. Nanayakkara, M. Challacombe, P.M.W. Gill, B. Johnson, W. Chen, M.W. Wong, C. Gonzalez, J.A. Pople, Gaussian 09 ed, Gaussian, Inc., Wallingford, 2008.
[28] M.A. Kurinovich, J.K. Lee, The acidity of uracil from the gas phase to solution: the coalescence of the N1 and N3 sites and implications for biological glycosylation, J. Am. Chem. Soc. 122 (2000) 6258–6262.
[29] M.T. Nguyen, A.K. Chandra, T. Zeegers-Huyskens, Protonation and deprotonation energies of uracil implications for the uracil–water complex, J. Chem. Soc. Faraday Trans. 94 (1998) 1277–1280.
[30] A.K. Chandra, M.T. Nguyen, T. Uchimaru, T. Zeegers-Huyskens, Protonation and deprotonation enthalpies of guanine and adenine and implications for the structure and energy of their complexes with water: comparison with uracil, thymine, and cytosine, J. Phys. Chem. A 103 (1999) 8853–8860.
[31] T.M. Miller, S.T. Arnold, A.A. Viggiano, A.E.S. Miller, Acidity of a nucleotide base: uracil, J. Phys. Chem. A 108 (2004) 3439–3446.
[32] Y.Q. Huang, H. Kenttamaa, Theoretical estimations of the 298 K gas-phase acidities of the pyrimidine-based nucleobases uracil, thymine, and cytosine, J. Phys. Chem. A 107 (2003) 4893–4897.
[33] M.A. Kurinovich, J.K. Lee, The acidity of uracil and uracil analogs in the gas phase: four surprisingly acidic sites and biological implications, J. Am. Soc. Mass Spectrom. 13 (2002) 985–995.
[34] T. Shimanouchi, Tables of molecular vibrational frequencies consolidated, Nat. Bur. Stand. 1 (1972) 1–164.
[35] E.A.L. Gillis, K. Rajabi, T.D. Fridgen, Structures of hydrated Li^{+}–thymine and Li^{+}–uracil complexes by IRMPD spectroscopy in the N–H/O–H stretching region, J. Phys. Chem. A 113 (2009) 824–832.
[36] E.A.L. Gillis, T.D. Fridgen, The hydrated Li^{+}–adenine–thymine complex by IRMPD spectroscopy in the N–H/O–H strtching region, Int. J. Mass Spectrom. 297 (2010) 2–8.
[37] K. Rajabi, E.A.L. Gillis, T.D. Fridgen, Structures of alkali metal ion-adenine complexes and hydrated complexes by IRMPD spectroscopy and electronic structure calculations, J. Phys. Chem. A 114 (2010) 3449–3456.
[38] M.F. Bush, R.J. Saykally, E.R. Williams, Hydration of the calcium dication: direct evidence for second shell formation from infrared spectroscopy, Chem. Phys. Chem. 8 (2007) 2245–2253.
[39] T. Pankewitz, A. Lagutschenkov, G. Niedner-Schatteburg, S.S. Xantheas, Y.T. Lee, Infrared spectrum of $NH_4^{+}(H_2O)$: evidence for mode specific fragmentation, J. Chem. Phys. 126 (2007) 74307–74321.